Thickness Effect on $(La_{0.26}Bi_{0.74})_2Ti_4O_{11}$ Thin-Film Composition and Electrical Properties *

Hui-Zhen Guo(郭会珍), An-Quan Jiang(江安全)**

State Key Laboratory of ASIC & System, School of Microelectronics, Fudan University, Shanghai 200433

(Received 25 October 2017)

Highly oriented (00l) $(La_{0.26}Bi_{0.74})_2Ti_4O_{11}$ thin films are deposited on (100) $SrTiO_3$ substrates using the pulsed laser deposition technique. The grains form a texture of bar-like arrays along $SrTiO_3$ ⟨110⟩ directions for the film thickness above 350 nm, in contrast to spherical grains for the reduced film thickness below 220 nm. X-ray diffraction patterns show that the highly ordered bar-like grains are the ensemble of two lattice-matched monoclinic $(La,Bi)_4Ti_3O_{12}$ and TiO_2 components above a critical film thickness. Otherwise, the phase decomposes into the random mixture of $Bi_2Ti_2O_7$ and $Bi_4Ti_3O_4$ spherical grains in thinner films. The critical thickness can increase up to 440 nm as the films are deposited on $LaNiO_3$-buffered $SrTiO_3$ substrates. The electrical measurements show the dielectric enhancement of the multi-components, and comprehensive charge injection into interfacial traps between $(La,Bi)_4Ti_3O_{12}$ and TiO_2 components occurs under the application of a threshold voltage for the realization of high-charge storage.

PACS: 68.65.−k, 77.80.−e, 77.84.−s, 67.80.dm DOI: 10.1088/0256-307X/35/2/026801

The Aurivillius-type $Bi_2Ti_4O_{11}$ compound was firstly synthesized by Subbarao that decomposed into TiO_2 and Bi-enriched phases ($Bi_4Ti_3O_{12}$ and $Bi_2Ti_2O_7$) at about 1225℃.[1] Its room-temperature crystal symmetry is monoclinic (space group $C2/c$) with lattice parameters of $a = 14.6412$ Å, $b = 3.8063$ Å, $c = 14.9418$ Å, and $\beta = 93.1288°$.[2,3] The *in-situ* studies using electron diffraction and electron microscopy suggested that antiferroelectric–paraelectric phase transition will occur at 508 K.[4] Similar antiferroelectric behavior was also observed in $x$$Bi_2Ti_4O_{11}$-$(1-x)$$Bi_4Ti_3O_{12}$ thin films (x is the ratio of the two phase compositions) through direct measurement of polarization versus electric field (P–E) hysteresis loops.[5] The additional data from dielectric and Raman studies coincidentally denoted that an additional phase transition in $Bi_2Ti_4O_{11}$ will occur at temperature comparable with the Curie point of ferroelectric $Bi_4Ti_3O_{12}$,[6–9] which predicts their correlation of phase structures.

Thin films with large dielectric constants have been the key issue for applications in microwave devices and dynamic random access memories. It has been found that dielectric constants of thin films decrease remarkably with the reduction of the film thickness due to the size effect.[10–13] To avoid this problem, a 'misfit-temperature' phase through the lattice-mismatched strains of thin films epitaxially grown on single-crystal substrates could provide the liability to tailor the dielectric functionality in a low-dimensional system,[14] especially desirable for the Aurivillius-type $Bi_2Ti_4O_{11}$ thin films with the coexistence of morphologic phase transitions.

Generally, La modification in bismuth-layered compounds can improve electrical performance of the devices. For example, $Bi_{3.25}La_{0.75}Ti_3O_{12}$ thin films have better fatigue property than $Bi_4Ti_3O_{12}$ at room temperature,[15] both electrical insulation and dielectric permittivity can be improved for La-modified $Bi_2Ti_2O_7$ thin films;[16] and the relative density can be increased from 92% to 98% with La modification of $Bi_2Ti_4O_{11}$ ceramics sintered between 900℃ and 1100℃.[9] In this Letter, we report the size effect and La modification on the misfit-temperature phase structure and crystallographic orientation of the Aurivillius-type $Bi_2Ti_4O_{11}$ thin films.

La-modified $Bi_2Ti_4O_{11}$ thin films were fabricated by the pulsed laser deposition (PLD) technique on (100) $SrTiO_3$ (STO) substrates at 750℃ with the oxygen pressure of 230 mTorr. A XeCl excimer laser beam with the wavelength of 308 nm and energy density of about 1.5 J/cm^2 at a 5 Hz repetition rate was focused onto a rotating ceramic $(La_{0.26}Bi_{0.74})_2Ti_4O_{11}$ (LBT) target. The advantage of PLD deposition is that it can faithfully transfer the right chemical composition to the films, and the La modification can improve the film crystallization in lowering of film leakage currents.[6,9] For electric characterization, a metallic $LaNiO_3$ (LNO) bottom layer with the thickness of 100 nm was previously deposited on STO under the identical condition. Here the lattice parameters of the $LaNiO_3$ buffer layer closely match with those of the STO substrate.[17,18] Top Pt electrodes were sputtered on the film surface at 500℃ through a shallow mask with areas of 3.1×10^{-4} cm^2. On- and off-axis x-ray diffraction (XRD) measurements were performed using a Rigaku diffractometer with a 12 kW rotating anode x-ray generator at the x-ray diffuse scatter-

*Supported by the Basic Research Project of Shanghai Science and Technology Innovation Action under Grant No 17JC1400300, the National Key Basic Research Program of China under Grant No 2014CB921004, the National Natural Science Foundation of China under Grant No 61674044, and the Program of Shanghai Subject Chief Scientist under Grant No 17XD1400800.

**Corresponding author. Email: aqjiang@fudan.edu.cn

© 2018 Chinese Physical Society and IOP Publishing Ltd

ing station of Beijing Synchrotron Radiation Facility (BSRF), where a synchroton radiation source near a Cu $K\alpha$ absorption line was used. The film chemical compositions were analyzed using an inductively coupled plasma emission spectrometer (ICP, Hitachi), and the film thicknesses were determined using a variable angle spectroscopic ellipsometer (GES5-E). The film morphology and roughness were investigated using an atomic force microscopy (AFM) in a contacting mode. Current transient versus time (I–t) data were calculated using a computer-controlled digital Keithley 2182 nanovoltmeter from the guidance of an instantaneous voltage drop across a 5 kΩ load resistor in series with the film capacitor. The dielectric capacitance and loss ($\tan\delta$) were measured using multi-frequency HP 4274 A and 4275 A impedance analyzers at room temperature. Polarization-electric field (P–E) hysteresis loops were measured using a Radiant RT6000s tester.

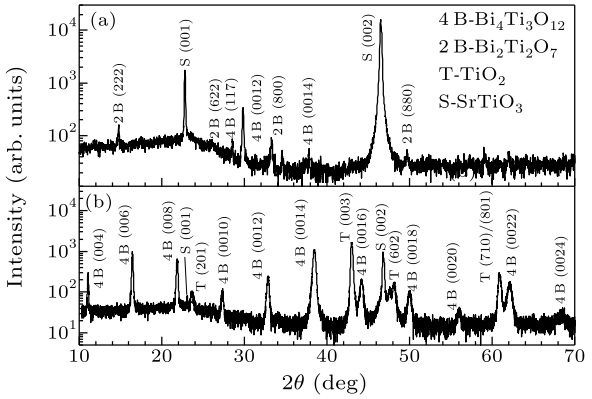

Fig. 1. XRD patterns for LBT/LNO/STO thin films with different thicknesses of (a) 300 nm and (b) 440 nm.

XRD patterns for LBT/LNO/STO thin films with different thicknesses are shown in Figs. 1(a) and 1(b). It is interesting to notice that the reflections in Fig. 1(a) with the film thickness of 300 nm are attributed to the perovskite $(La,Bi)_4Ti_3O_{12}$ and pyrochlore $(La,Bi)_2Ti_2O_7$ phases, where the $(La,Bi)_4Ti_3O_{12}$ component has a preferential (117) orientation. Once the film thickness is increased up to 440 nm, the reflections in Fig. 1(b) show the coexistence of the monoclinic $(La,Bi)_4Ti_3O_{12}$ and TiO_2 (space group $C2/m$) components different from those in Fig. 1(a). These results indicate $Bi_2Ti_4O_{11}$ phase decomposition in thin films and phase transformation of the components with the increase of the film thickness. Normally, the $Bi_2Ti_4O_{11}$ phase decomposition should occur at high temperature of 1225℃.[1] However, the appearance of misfit-temperature phases here through the reduction of film thickness reveals the breaking of the energy balance between grain surfaces and lattice-mismatched strain fields for the $(La,Bi)_2Ti_4O_{11}$. The lattice-mismatched strains seemingly vary with the film thickness that promotes the intermediate phase transformation during the growth of bismuth-layered compounds. It was experimentally proved that the intermediate $Bi_2Ti_2O_7$ phase could transfer into $Bi_4Ti_3O_{12}$ during the growth of the film.[9,19,20] The lattice parameters for the monoclinic symmetry in the bulk are $a = 12.17$ Å, $b = 3.741$ Å, $c = 6.524$ Å, and $\beta = 107.05°$ for TiO_2,[21] while $a = 5.442$ Å, $b = 5.421$ Å, $c = 32.713$ Å, and $\beta = 90°$ for $Bi_4Ti_3O_{12}$.[22] Here the out-of-plane spacing of each component is $c = 32.97 \pm 0.02$ Å for $(La,Bi)_4Ti_3O_{12}$ but $c \cdot \sin\beta = 6.17 \pm 0.02$ Å for TiO_2 in Fig. 1(b) that are slightly elongated and shortened in comparison with their bulk crystals, respectively.

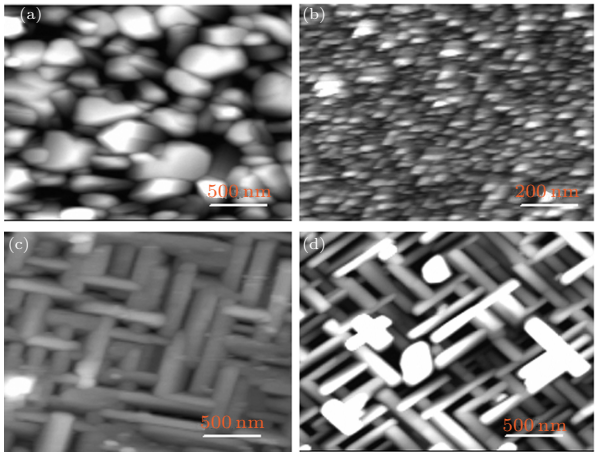

Fig. 2. AFM micrographs for LBT/LNO/STO with film thicknesses of (a) 300 nm and (b) 440 nm, and for LBT/STO with film thicknesses of (c) 220 nm and (d) 350 nm.

AFM micrographs are shown for either LBT/LNO/STO in Figs. 2(a) and 2(b) or LBT/STO in Figs. 2(c) and 2(d) with various film thicknesses. The films in Figs. 2(b) and 2(d) show regular arrays of bar-like grains aligned along two perpendicular ⟨110⟩ directions of STO substrates, unlike typical plate-like $Bi_4Ti_3O_{12}$ and granular TiO_2 films.[23–25] Instead, all grains exhibit a typical growing habit of needle-like $Bi_2Ti_4O_{11}$ single crystals.[26] From XRD patterns in Fig. 1(b), we can realize that each bar-like grain is in fact the mixture of TiO_2 and $(La,Bi)_4Ti_3O_{12}$ components. As the film thickness decreases below a critical value of 440 nm in Fig. 2(a) but 220 nm in Fig. 2(c), the films are the ensemble of two kinds of spherical grains (one is larger, and the other is smaller), giving rise to the phase decomposition into $(La,Bi)_4Ti_3O_{12}$ and $(La,Bi)_2Ti_2O_7$ constituents, as shown in Figs. 1(a). It seems that the LNO buffer layer increases the critical film thickness. AFM observation of the LNO buffer layer shows a spherical grain shape that could enhance the lattice-mismatched stresses and could slow lateral diffusion of chemical elements for the formation of the $(La,Bi)_2Ti_4O_{11}$ crystallites during the film deposition. In contrast, the atomic smoothness of $SrTiO_3$ substrates can promote lateral element diffusion in lowering of the above crystalized energy.

In-plane θ–2θ and azimuthal (ϕ) scans of reflections by the small-angle (∼0.3°). X-ray graz-

ing incidence for the 350-nm-thickLBT/STO thin film reveals an epitaxial relationship of $Bi_4Ti_3O_{12}$ [100]/[010]//TiO_2 [100] with a misaligned angle of ∼1.01°. The ϕ scan in Fig. 3(a) gives the TiO_2 ($\bar{6}01$) fundamental peak that periodically appears at $\phi = 0°$, 90°, and 180°. In contrast, θ–2 θ scanning of $(La,Bi)_4Ti_3O_{12}$ (200)/(020) fundamental peaks in Fig. 3(b) yields in-plane lattice constants of $Bi_4Ti_3O_{12}$ with $a \approx b = 5.40 \pm 0.02$ Å. These peaks are broad, which suggests the overlapping of (200) and (020) or (400) and (040) fundamental peaks and manifest a monoclinic phase symmetry ($a \neq b$).

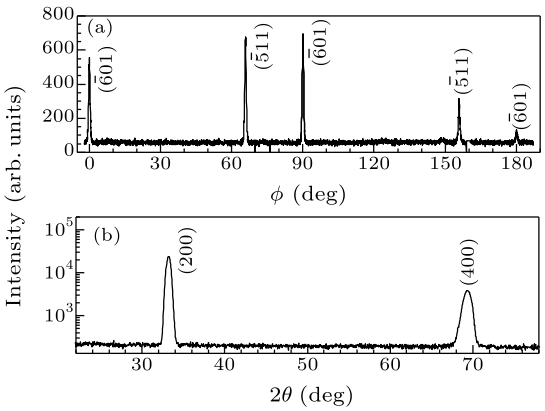

Fig. 3. In-plane Φ scan of (a) monoclinic TiO_2 and θ–2θ scan of (b) monoclinic $Bi_4Ti_3O_{12}$ fundamental peaks for 350 nm LBT/STO thin film.

Generally, $Bi_4Ti_3O_{12}$ is orthorhombic at room temperature and its Raman modes are broad.[27] A phase transition into the monoclinic symmetry could occur in the temperature range of 150–200 K, accompanied by narrowing of its discrete Raman lines.[28,29] Simultaneously, the monoclinic TiO_2 could be synthesized by the hydrolysis of $K_2Ti_4O_9$ at 500℃.[30] However, the subsequent phase transformation into the anatase immediately occurs between 600 and 700℃. It seems that the discrete monoclinic TiO_2 phase is unstable at 750℃ during the film deposition below a critical film thickness. With the formation of the bar-like grains in a thicker film, the two kinds of grains of monoclinic $(La,Bi)_4Ti_3O_{12}$ and monoclinic TiO_2 can coexist due to the lattice-mismatched stresses which order alternately along STO ⟨110⟩ directions. The interplaner spacing of $\sqrt{2}a$ ($a = 3.90$ Å) matches the a/b constants of the $(La,Bi)_4Ti_3O_{12}$ component in minimizing surface and strain energies of the grains, and thus the misfit-temperature phases of the two monoclinic components are stabilized.[14]

The frequency dependence of dielectric response for Pt/LBT/LNO/STO thin-film capacitors with different thicknesses is shown in Fig. 4. The dielectric constant ε is 80 for the 440-nm-thick film that shows slight dispersion with the frequency in the range of 1–100 MHz. However, ε increases up to 108 at 100 Hz with the reduction of the film thickness to 300 nm, as shown in Fig. 4. This value decreases to 88 with further enhanced frequency up to 200 kHz. Meanwhile, the dielectric loss is also increased. This dielectric enhancement in thin films with the random mixture of two kinds of spherical grains seemingly originates from the interfacial Maxwell–Wager relaxation.[31]

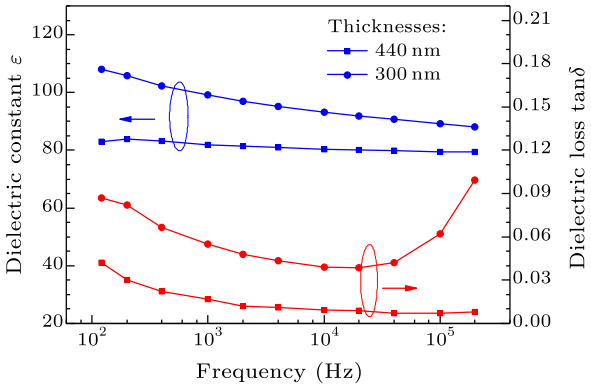

Fig. 4. Frequency dependence of the dielectric response for Pt/LBT/LNO/STO thin-film capacitors with different thicknesses.

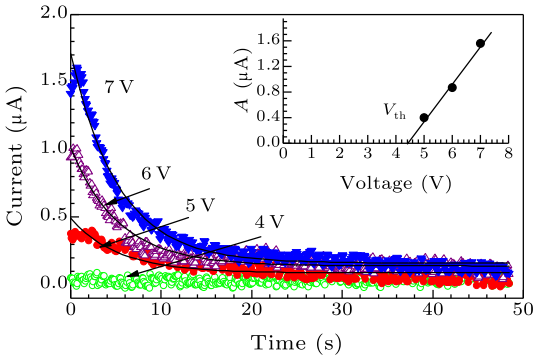

Fig. 5. The I–t curves for 440 nm Pt/LBT/LNO/STO thin-film capacitors under applications of various positive voltages. The film is pre-polarized under −7 V for 3 min before each measurement. The solid lines are the best fitting of the data in accordance with Eq. (1). The inset shows the V_{appl} dependence of extracted parameter A.

Figure 5 shows the I–t measurements of the 440 nm-thick LBT/LNO/STO thin-film capacitor under applications of various positive voltages to the bottom electrode, where the top electrode is grounded. Initially, the current transients of a fresh sample exhibit the Barhausen noise with the appearance of many sharp current peaks,[32] which can be attributed to the inhomogeneity of avalanche-like charge injection into the interfaces between two heterogeneous $(La,Bi)_4Ti_3O_{12}$ and TiO_2 components.[33] However, the noise disappears from the I–t curve in Fig. 5 after poling at +/−7 V for a few tens of cycles. After that, the capacitor was pre-polarized under −7 V for 3 min, and then discharged by short-circuiting of top and bottom electrodes for 1 s before each measurement. The overall current transients at voltages higher than 5 V are similar to capacitor charging, and can be described by

$$I = A \exp\left(-\frac{t}{\tau_0}\right) + B, \qquad (1)$$

where τ_0 is the relaxation time, and A and B are constants depending on the applied voltage $V_{\rm appl}$. The solid lines in Fig. 5 are the best fitting of the data in accordance with Eq. (1) that gives $\tau_0 = 5.3$ s. It is obvious that τ_0 is far larger than the circuit RC-time constant of 245 ns. As we repeated these measurements without pre-poling of the capacitor at -7 V, there is no charging current, either, as $V_{\rm appl}$ is below 4 V, the charging current disappears from Fig. 5. Therefore, these charging currents should be correlated with the slow ferroelectric domain switching of the $(La,Bi)_4Ti_3O_{12}$ constituent. Figure 6 shows the P–E hysteresis loop under application of a triangular wave with different frequencies. The P–E hysteresis loop is almost linear at 67 Hz, in agreement with Subbarao's observation in the bulk ceramics.[1] However, this loop becomes almost squared with lowering of the frequency to 5 Hz (the rounded corners of the loop suggest the contribution of the involved space charge injection).

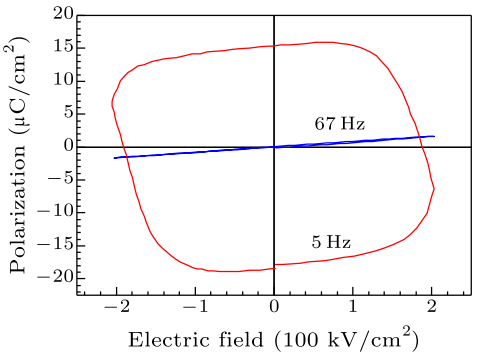

Fig. 6. The P–E hysteresis loop at frequencies of 67 Hz and 5 Hz for the 440-nm-thick Pt/LBT/LNO/STO thin-film capacitors.

Each bar-like LBT grain contains both $(La,Bi)_4Ti_3O_{12}$ and TiO_2 components with volumes of 967.30 Å^3 and 284.23 Å^3 and densities of 8.045 g/cm and 1.867 g/cm for their primitive cells, respectively. The two components could grow alternately along the $(La,Bi)_4Ti_3O_{12}$ [100]/[010] direction. The total thickness ratio of the two components would be 0.6806 to satisfy an average molecular formula of $(La,Bi)_2Ti_4O_{11}$.

A genuine film texture along the $(00l)$ orientation should be the random pileup of in-plane ordered bar-like grains. As the film thickness and the electrode size are far larger than the radial size of the bar-like grain, electrical properties of the composite can be equivalently described in terms of two TiO_2 (TO) and $(La,Bi)_4Ti_3O_{12}$ (LBT) sublayers connected in series with layer thicknesses of $d_{\rm i}$ and $d_{\rm f}$ ($d_{\rm f}/d_{\rm i} = 0.6806$), respectively. From the continuum dielectric equations, we have

$$\frac{d}{\varepsilon} = \frac{d_{\rm i}}{\varepsilon_{\rm i}} + \frac{d_{\rm f}}{\varepsilon_{\rm f}}, \ (d = d_{\rm i} + d_{\rm f}), \tag{2}$$

$$V_{\rm appl} = d_{\rm i}E_{\rm i} + d_{\rm f}E_{\rm f}, \tag{3}$$

$$D_{\rm i}(t) = \varepsilon_0\varepsilon_{\rm i}E_{\rm i}(t), \tag{4}$$

$$D_{\rm f}(t) = \varepsilon_0\varepsilon_{\rm f}E_{\rm f}(t) + P_{\rm s}, \tag{5}$$

$$J(t) = \sigma_{\rm i} + \frac{\partial D_{\rm i}(t)}{\partial t} = \sigma_{\rm f} + \frac{\partial D_{\rm f}(t)}{\partial t}, \tag{6}$$

where $E_{\rm i}$ ($E_{\rm f}$) and $D_{\rm i}$ ($D_{\rm f}$) are the field and dielectric displacement across the TO (LBT) layer, respectively, ε_0 is the vacuum permittivity, $P_{\rm s}$ is the saturation polarization of the LBT layer, $J(t)$ is the current density of the film, and $\sigma_{\rm i}$ ($\sigma_{\rm f}$) is the electric conductivity of the TO (LBT) layer. From the assumption of $\varepsilon_{\rm f} = 140$ for the c-oriented LBT,[34] the dielectric constant for the monoclinic TiO_2 is calculated to be 61 according to Eq. (2), slightly higher than 50 for the anatase TiO_2.[24,25] In equilibrium as $t = 0$ and $V_{\rm appl} = 0$, the interfacial trapped charge density for a fully compensated polarized thin film between TO and LBT layers is $\pm P_{\rm s}$. From Eqs. (3)–(6), we derive

$$E_{\rm i} = \Big[\Big(\frac{\varepsilon_0\varepsilon_{\rm f}}{\varepsilon_0\varepsilon_{\rm i}d_{\rm f} - \varepsilon_0\varepsilon_{\rm f}d_{\rm i}} - \frac{\sigma_{\rm f}}{\sigma_{\rm i}d_{\rm f} + \sigma_{\rm f}d_{\rm i}}\Big)V_{\rm appl} + \frac{2P_{\rm s}d_{\rm f}}{\varepsilon_0\varepsilon_{\rm i}d_{\rm f} + \varepsilon_0\varepsilon_{\rm f}d_{\rm i}}\Big] \exp\Big(-\frac{\sigma_{\rm i}d_{\rm f} + \sigma_{\rm f}d_{\rm i}}{\varepsilon_0\varepsilon_{\rm i}d_{\rm f} + \varepsilon_0\varepsilon_{\rm f}d_{\rm i}}t\Big) + \frac{\sigma_{\rm f}}{\sigma_{\rm i}d_{\rm f} + \sigma_{\rm f}d_{\rm i}}V_{\rm appl}, \tag{7}$$

$$J(t) = \Big(\sigma_{\rm i} - \frac{\varepsilon_{\rm i}d_{\rm f}\sigma_{\rm i} + \varepsilon_{\rm i}d_{\rm i}\sigma_{\rm f}}{\varepsilon_{\rm i}d_{\rm f} + \varepsilon_{\rm f}d_{\rm i}}\Big)\Big[\Big(\frac{\varepsilon_0\varepsilon_{\rm f}}{\varepsilon_0\varepsilon_{\rm i}d_{\rm f} - \varepsilon_0\varepsilon_{\rm f}d_{\rm i}} - \frac{\sigma_{\rm f}}{\sigma_{\rm i}d_{\rm f} + \sigma_{\rm f}d_{\rm i}}\Big)V_{\rm appl} + \frac{2P_{\rm s}d_{\rm f}}{\varepsilon_0\varepsilon_{\rm i}d_{\rm f} + \varepsilon_0\varepsilon_{\rm f}d_{\rm i}}\Big] \cdot \exp\Big(-\frac{\sigma_{\rm i}d_{\rm f} + \sigma_{\rm f}d_{\rm i}}{\varepsilon_0\varepsilon_{\rm i}d_{\rm f} + \varepsilon_0\varepsilon_{\rm f}d_{\rm i}}t\Big) + \frac{\sigma_{\rm i}\sigma_{\rm f}}{\sigma_{\rm i}d_{\rm f} + \sigma_{\rm f}d_{\rm i}}V_{\rm appl}, \tag{8}$$

where $E_{\rm f}$ will increase gradually with t under the application of $V_{\rm appl}$ along with the ongoing charge injection. Once $E_{\rm f}$ is increased over the coercive field of ferroelectric domain switching, the polarization reversal within the LBT constituent would occur, and thus we can observe current transients in Fig. 5 and a squared P–E hysteresis loop at 5 Hz in Fig. 6. The charge injection of ferroelectric domain switching reduces quickly with the increase of the frequency, and the domains become unswitched as $t < \tau_0$, thus P–E is almost linear at 67 Hz in Fig. 6. From the comparison of Eq. (8) with Eq. (1), we obtain

$$A = \Big(\sigma_{\rm i} - \frac{\varepsilon_{\rm i}d_{\rm f}\sigma_{\rm i} + \varepsilon_{\rm i}d_{\rm i}\sigma_{\rm f}}{\varepsilon_{\rm i}d_{\rm f} + \varepsilon_{\rm f}d_{\rm i}}\Big) \times \Big[\Big(\frac{\varepsilon_0\varepsilon_{\rm f}}{\varepsilon_0\varepsilon_{\rm i}d_{\rm f} - \varepsilon_0\varepsilon_{\rm f}d_{\rm i}} - \frac{\sigma_{\rm f}}{\sigma_{\rm i}d_{\rm f} + \sigma_{\rm f}d_{\rm i}}\Big)V_{\rm appl} + \frac{2P_{\rm s}d_{\rm f}}{\varepsilon_0\varepsilon_{\rm i}d_{\rm f} + \varepsilon_0\varepsilon_{\rm f}d_{\rm i}}\Big], \tag{9}$$

$$\tau_0 = \frac{\varepsilon_0\varepsilon_{\rm i}d_{\rm f} + \varepsilon_0\varepsilon_{\rm f}d_{\rm i}}{\sigma_{\rm i}d_{\rm f} + \sigma_{\rm f}d_{\rm i}}, \tag{10}$$

$$B = \frac{\sigma_{\rm i}\sigma_{\rm f}}{\sigma_{\rm i}d_{\rm f} + \sigma_{\rm f}d_{\rm i}}V_{\rm appl}. \tag{11}$$

Equation (9) predicts a linear plot of A versus $V_{\rm appl}$ that will pass through the origin if $P_{\rm s} = 0$. Otherwise, the above plot would intercept with the voltage axis at

a threshold voltage $V_{\rm th}$ below which the ferroelectric polarization is unswitched,

$$V_{\rm th} = \frac{2P_{\rm s}(\sigma_{\rm i}d_{\rm f} + \sigma_{\rm f}d_{\rm i})}{\varepsilon_0\varepsilon_{\rm i}\sigma_{\rm f} - \varepsilon_0\varepsilon_{\rm f}\sigma_{\rm i}}. \quad (12)$$

Finally, the $V_{\rm appl}$ dependence of A derived from the data fitting of current transients in accordance with Eq. (1) is shown in the inset of Fig. 5. The plot can be fitted by the solid line in accordance with Eq. (9). The line intercepts with the voltage axis at $V_{\rm th}$ of 4.4 V ($P_{\rm s} \neq 0$) in prediction of the appearance of ferroelectricity for the $(La,Bi)_4Ti_3O_{12}$ component. As $V_{\rm appl} < 4.4$ V, the domains are hardly switched, in agreement with the observations of the absence of charging current transients under $V_{\rm appl} \leq 4$ V in Fig. 5.

In summary, the La-modified $Bi_2Ti_4O_{11}$ thin film above a critical thickness contains two lattice-matched monoclinic TiO_2 and $(La,Bi)_4Ti_3O_{12}$ components along the $(La,Bi)_4Ti_3O_{12}$ [100]/[010] directions, where the grains show a highly ordered bar-like texture. Below a critical film thickness, the bar-like grains decomposed into two kinds of $(La,Bi)_4Ti_3O_{12}$ and $(La,Bi)_2Ti_2O_7$ spherical grains. The morphologic phase transformation is similar to the high-temperature sintering of $(La,Bi)_4Ti_3O_{12}$ and $(La,Bi)_2Ti_4O_{11}$ ceramics.[6,9] The $(La,Bi)_4Ti_3O_{12}$ component is ferroelectric, as implicated from two-layer modeling of current transients with time. Comprehensive longtime charge injection into two component interfaces occurs above a coercive voltage along with ferroelectric domain switching.

References

[1] Subbarao E C 1962 *J. Am. Ceram. Soc.* **45** 564
[2] Kahlenberg V and Bohm H 1994 *J. Phys.: Condens. Matter* **6** 6221
[3] Kahlenberg V and Bohm H 1995 *Acta Crystallogr. Sect.* B **51** 11
[4] Buscaglia M T, Sennour M, Buscaglia V, Bottino C, Kalyani V and Nanni P 2011 *Cryst. Growth Des.* **11** 1394
[5] Jiang A Q, Cheng Z H, Cheng F, Zhou Y L, He M and Yang G Z 2001 *Phys. Rev.* B **63** 104102
[6] Jiang A Q, Hu Z X and Zhang L D 1999 *J. Appl. Phys.* **85** 1739
[7] Liu J, Duan C G, Yin W G, Mei W N, Smith R W and Hardy J R 2003 *J. Chem. Phys.* **119** 2812
[8] Meng J F, Katiyar R S and Zou G T 1997 *J. Raman Spectrosc.* **28** 797
[9] Jiang A Q, Hu Z X and Zhang L D 1999 *Appl. Phys. Lett.* **74** 114
[10] Black C T and Welser J J 1999 *IEEE Trans. Electron Devices* **46** 776
[11] Hardy A, D'Haen J, Goux L, Dirk, Marlies, Rul H V and Mullens J 2007 *Chem. Mater.* **19** 2994
[12] Lee B T and Hwang C S 2000 *Appl. Phys. Lett.* **77** 124
[13] Vendik O G, Zubko S P and Ter-Martirosayn L T 1998 *Appl. Phys. Lett.* **73** 37
[14] Pertsev N A, Zembilgotov A G and Tagantsev A K 1998 *Phys. Rev. Lett.* **80** 1988
[15] Park B H, Kang B S, Bu S D, Noh T W, Lee J and Jo W 1999 *Nature* **401** 682
[16] Yang X N, Huang B B, Wang H B, Shang S H, Yao W F and Wei J Y 2004 *J. Cryst. Growth* **270** 98
[17] Mizutani Y, Kiguchi T, Konno T J, Funakubo H and Uchida H 2010 *Jpn. J. Appl. Phys.* **49** 09MA02
[18] Chu C M and Lin P 1997 *Appl. Phys. Lett.* **70** 249
[19] Nakamura T, Muhammet R, Shimizu M and Shiosaki T 1993 *Jpn. J. Appl. Phys. Part.* **32** 4086
[20] Merka O, Bahnemann D W and Wark M 2014 *Catal. Today* **225** 102
[21] Borghols W J H, Wagemaker M, Lafont U, Kelder E M and Mulder F M 2008 *Chem. Mater.* **20** 2949
[22] Lardhi S, Noureldine D, Harb M, Ziani A, Cavallo L and Takanabe K 2016 *J. Chem. Phys.* **144** 134702
[23] Theis C D, Yeh J, Schlom D G, Hawley M E, Brown G W, Jiang J C and Pan X Q 1998 *Appl. Phys. Lett.* **72** 2817
[24] Shin H, De Guire M R and Heuer A H 1998 *J. Appl. Phys.* **83** 3311
[25] Ha H K, Yoshimoto M, Koinuma H, Moon B K and Ishiwara H 1996 *Appl. Phys. Lett.* **68** 2965
[26] Shimada S, Kodaira K and Matsushita T 1977 *J. Cryst. Growth* **41** 317
[27] Dobal P S and Katiyar R S 2002 *J. Raman Spectrosc.* **33** 405
[28] Idink H, Srikanth V, White W B and Subbarao E C 1994 *J. Appl. Phys.* **76** 1819
[29] Wu Y, Zhang D, Yu J and Wang Y 2009 *Mater. Chem. Phys.* **113** 422
[30] Marchand R, Brohan L and Tournoux M 1980 *Mater. Res. Bull.* **15** 1129
[31] Shen M R, Ge S B and Cao W W 2001 *J. Phys.* D **34** 2935
[32] Jiang A Q, Chen Z H, Zhou Y L and Yang G Z 2001 *Solid State Commun.* **120** 65
[33] Csikor F F, Motz C, Weygand D, Zaiser M and Zapperi S 2007 *Science* **318** 251
[34] Fouskova A and Cross L E 1970 *J. Appl. Phys.* **41** 2834